Supporting Information for

A New Strategy for Achieving High K^+ Storage Capacity with Fast Kinetics: Realizing Covalent Sulfur-Rich Carbon by Phosphorous Doping

Wenrui Wei,[a] Yulong Zheng,[c] Minghua Huang,[a] Jing Shi,[a] Lei Li,[b] Zhicheng Shi,[a] Shuai Liu[a] and Huanlei Wang[a*],

[a] *School of Materials Science and Engineering, Ocean University of China, Qingdao 266100, People's Republic of China.*

[b] *Key Laboratory of Extraordinary Bond Engineering and Advanced Materials Technology (EBEAM) of Chongqing, Yangtze Normal University, Chongqing 408100, People's Republic of China.*

[c] *New Energy R&D Center/New Energy Powertrain Dept, Weichai Power Co.,Ltd, Weifang 261061, People's Republic of China*.

[*]Corresponding author.

E-mail:huanleiwang@gmail.com (Prof. H. Wang)

Figures

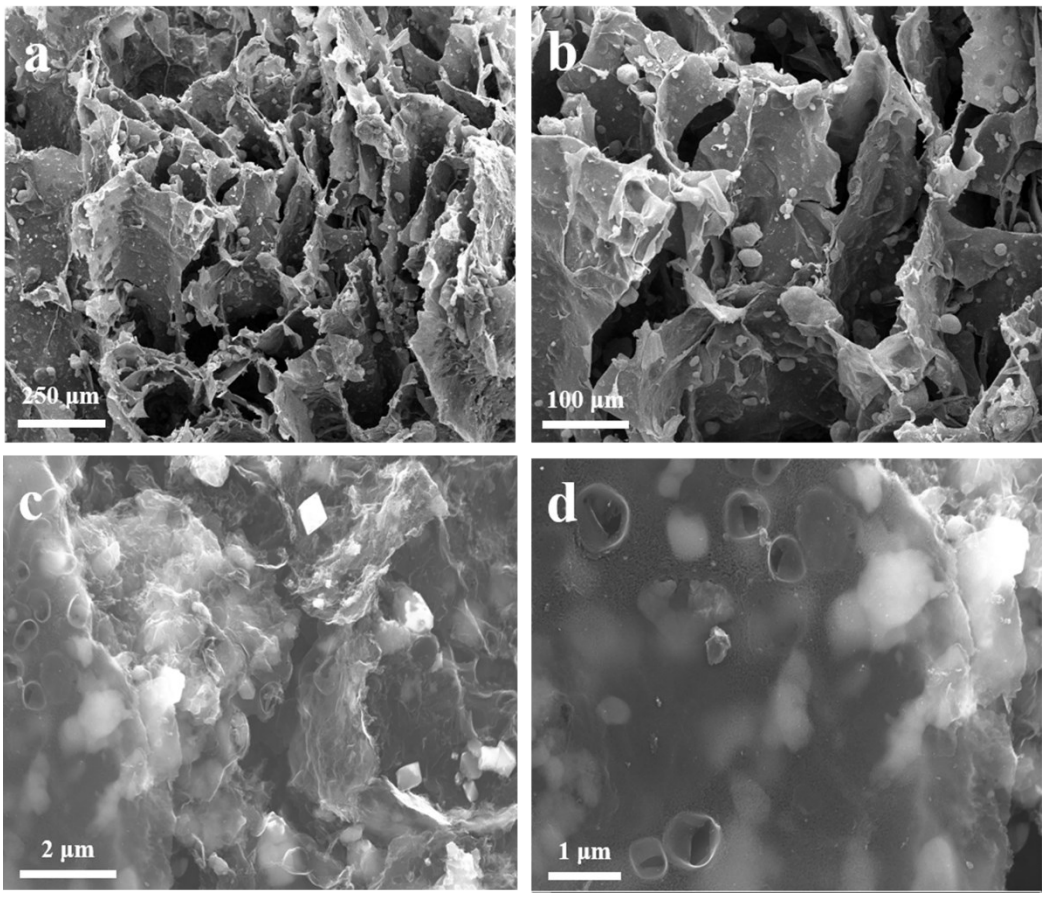

Fig. S1 Representative SEM image of (a, b) magnesium phosphate pentahydrate dispersed in carrageenan, and (c,d) the PSMC sample before washing with HCl.

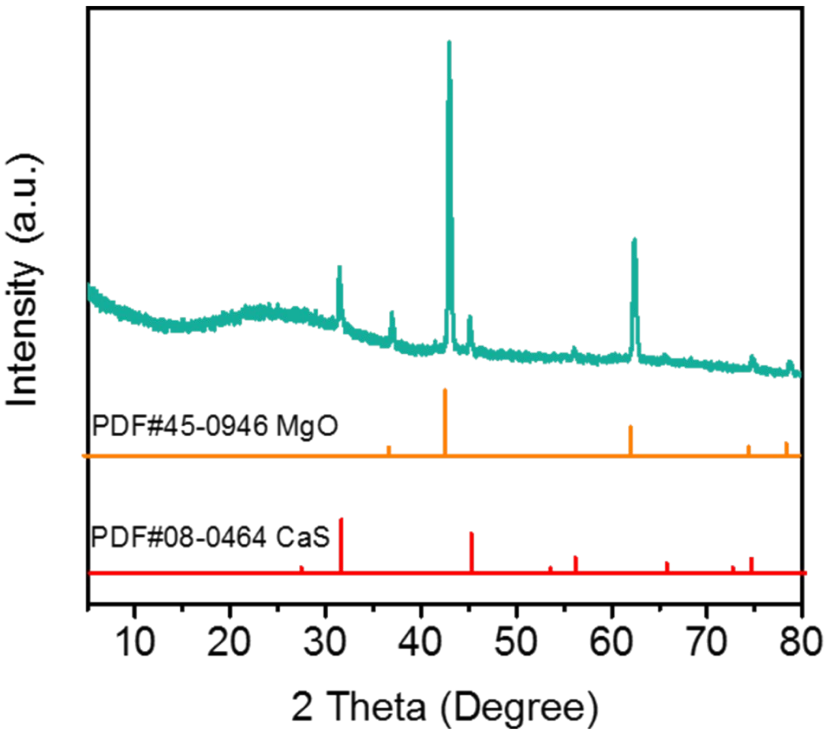

Fig. S2 The XRD pattern of PSMC without acid-treatment. (As evidenced in the XRD spectrum, the generation of MgO is due to the decomposition of magnesium phosphate pentahydrate during the carbonization process at 1200°C. There is ester-sulfate and a slight amount of Ca^{2+} in carrageenan, the decomposition of ester-sulfate achieved S-doped while partially binding with Ca^{2+} to form CaS.[1])

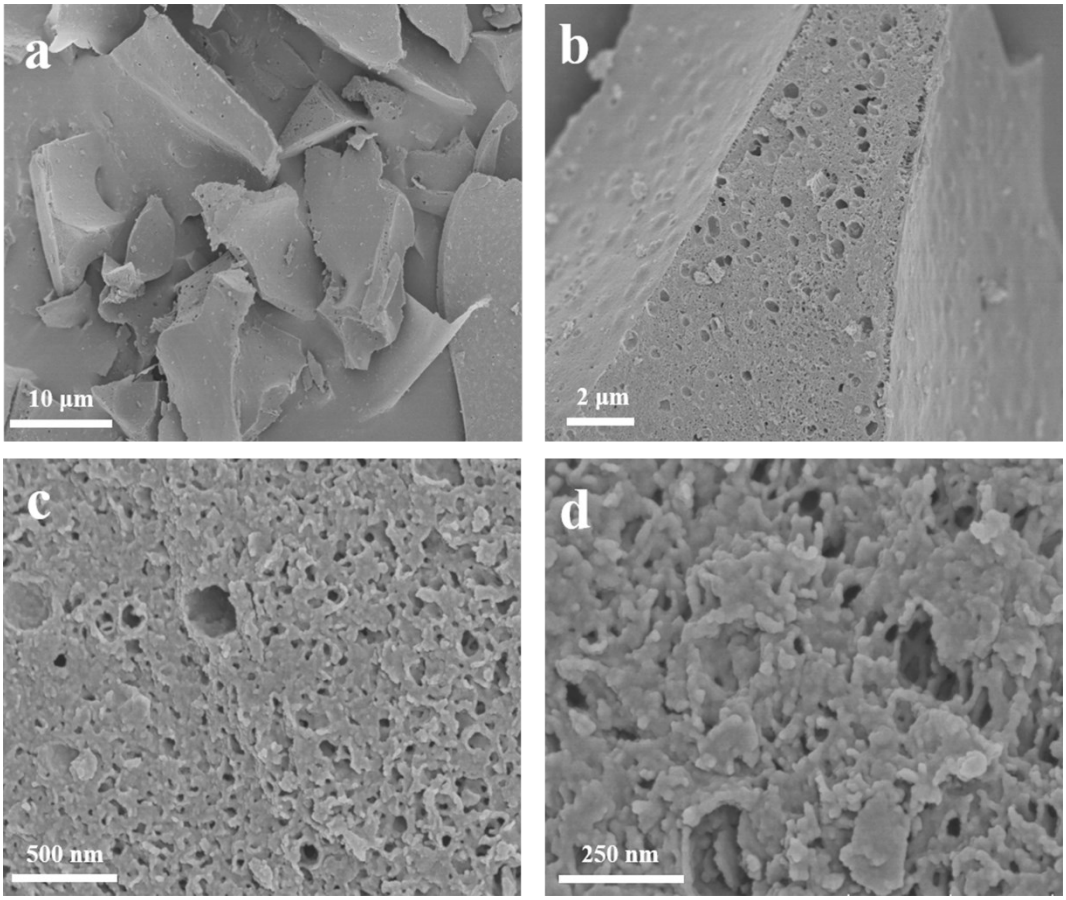

Fig. S3 Representative SEM images of SMC.

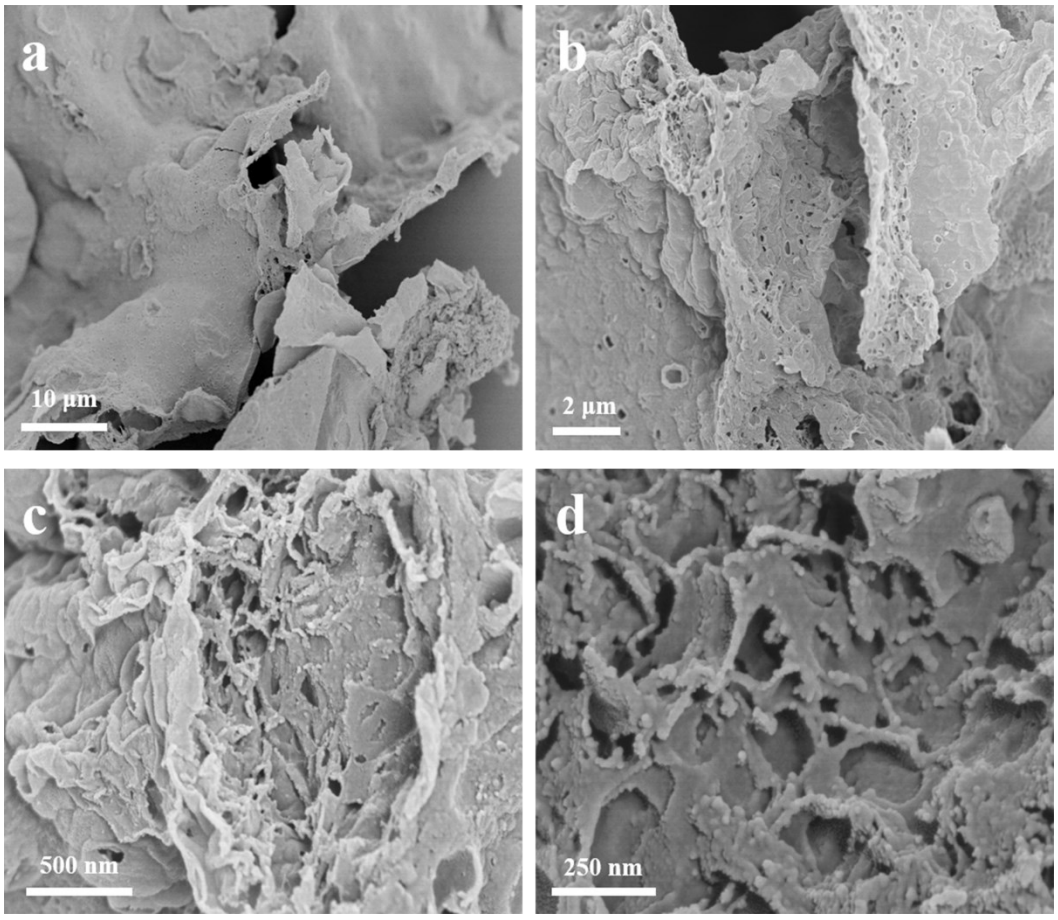

Fig. S4 Representative SEM images of PSMC.

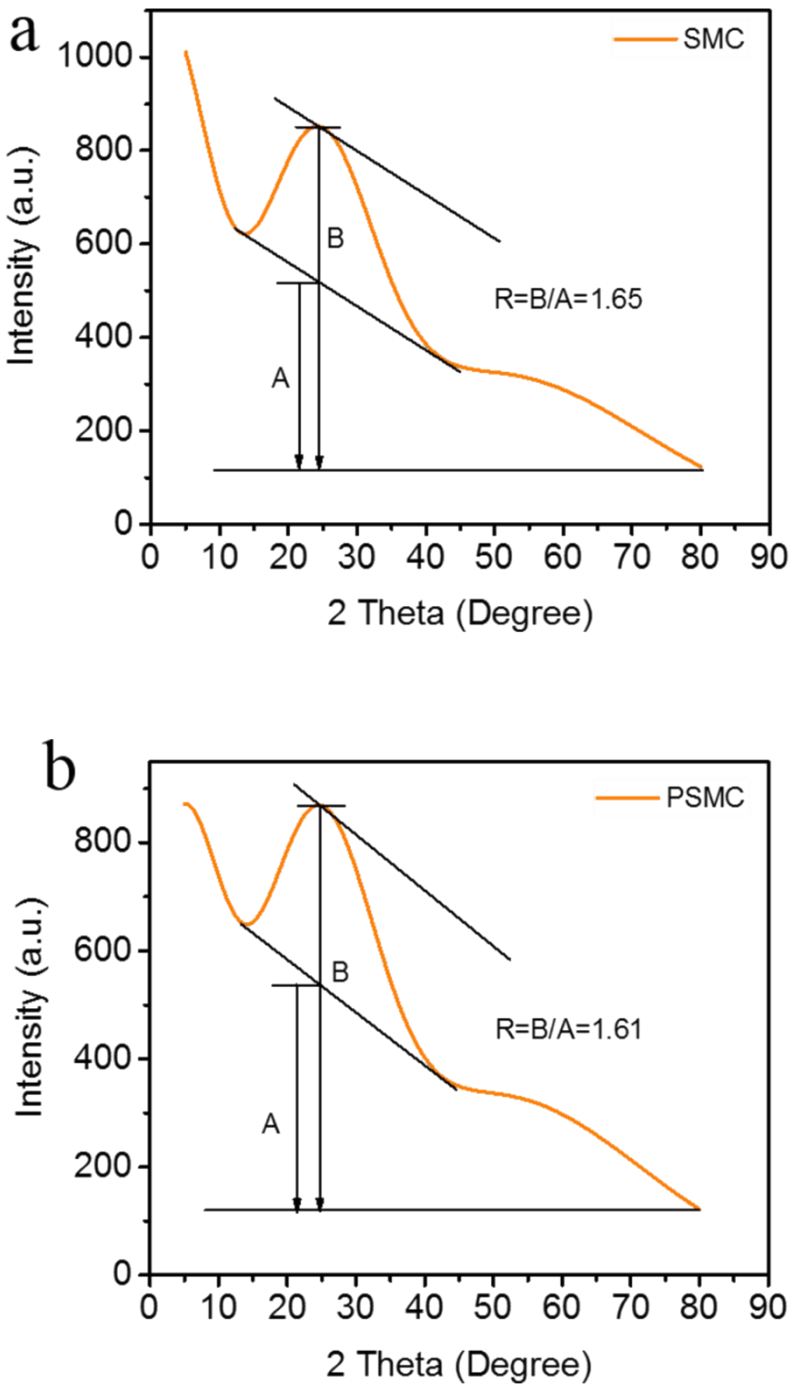

Fig. S5 Scheme illustrating the calculation of R values based on XRD patterns for (a) SMC and (b) PSMC.

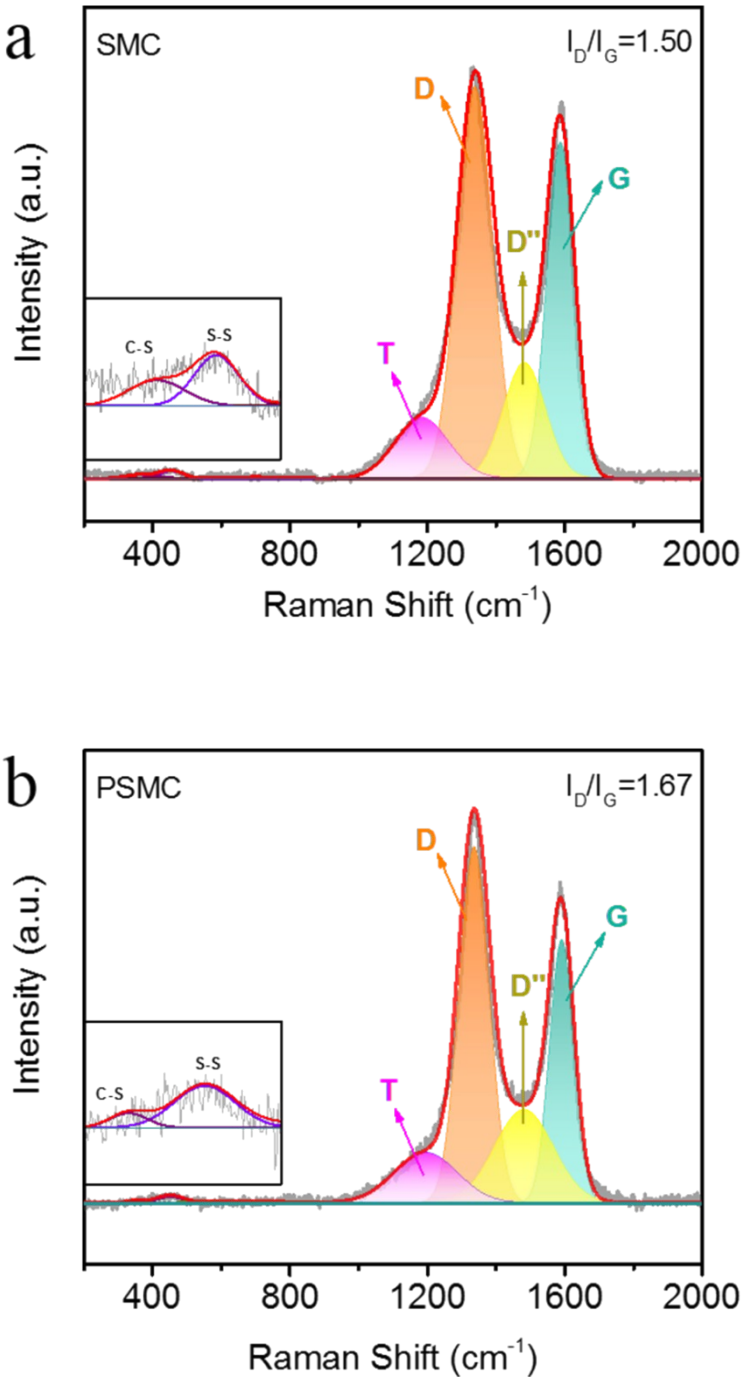

Fig. S6 Curve fitting results for the Raman spectra of (a) SMC and (b) PSMC.

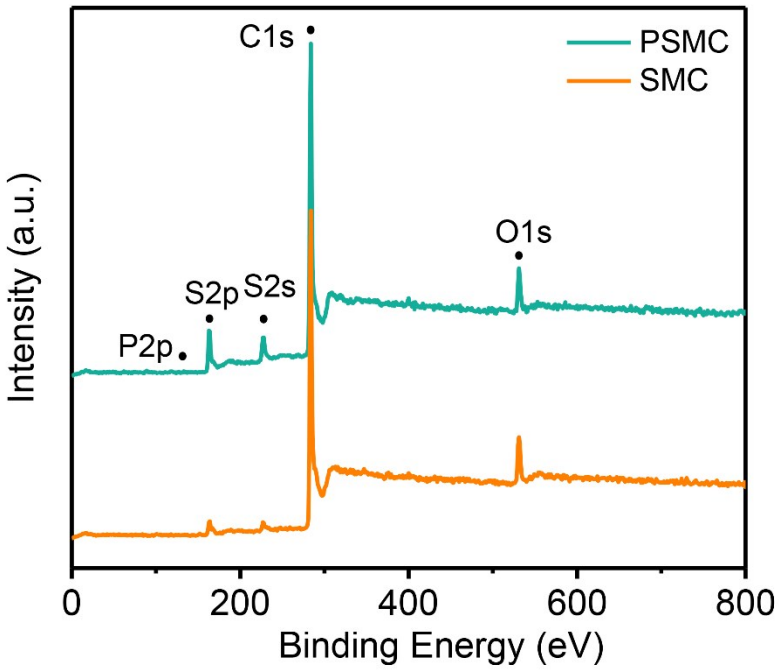

Fig. S7 The XPS survey spectra of SMC and PSMC.

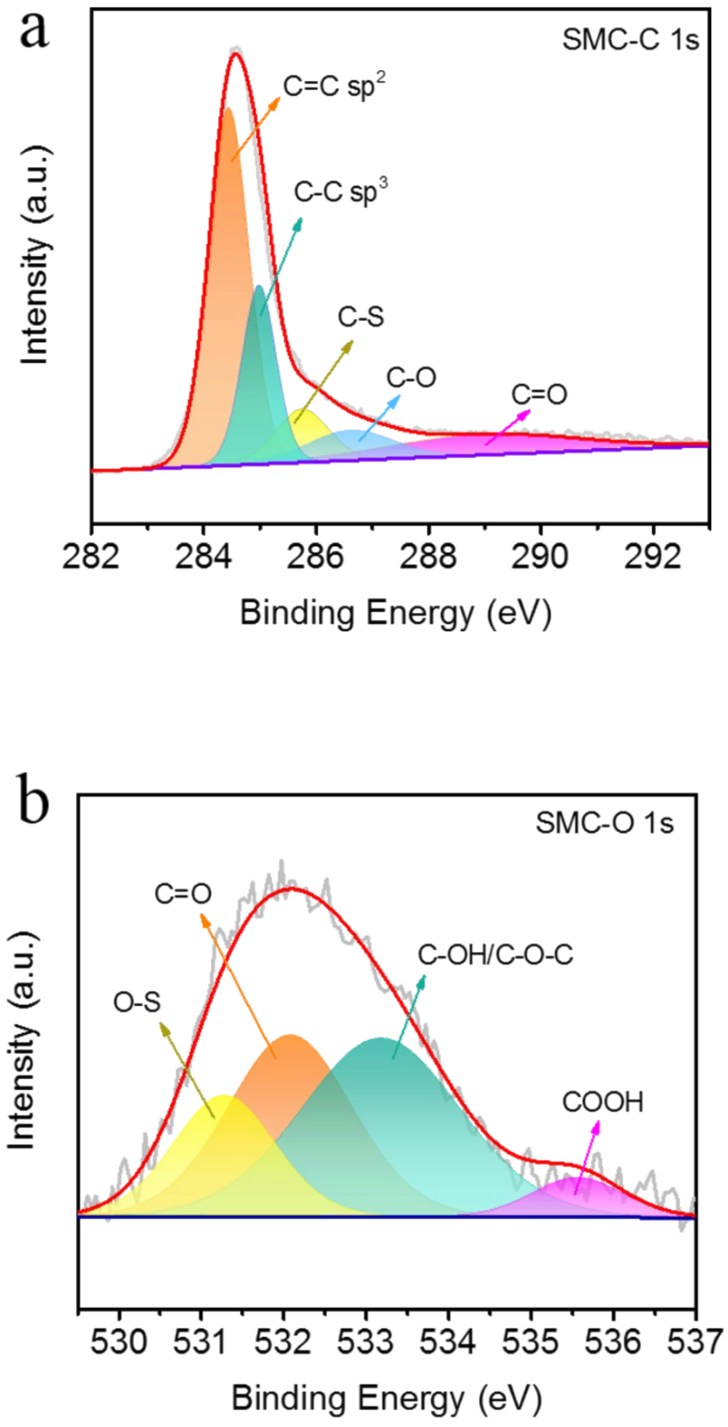

Fig. S8 High-resolution (a) C 1s and (b) O 1s XPS spectra for SMC.

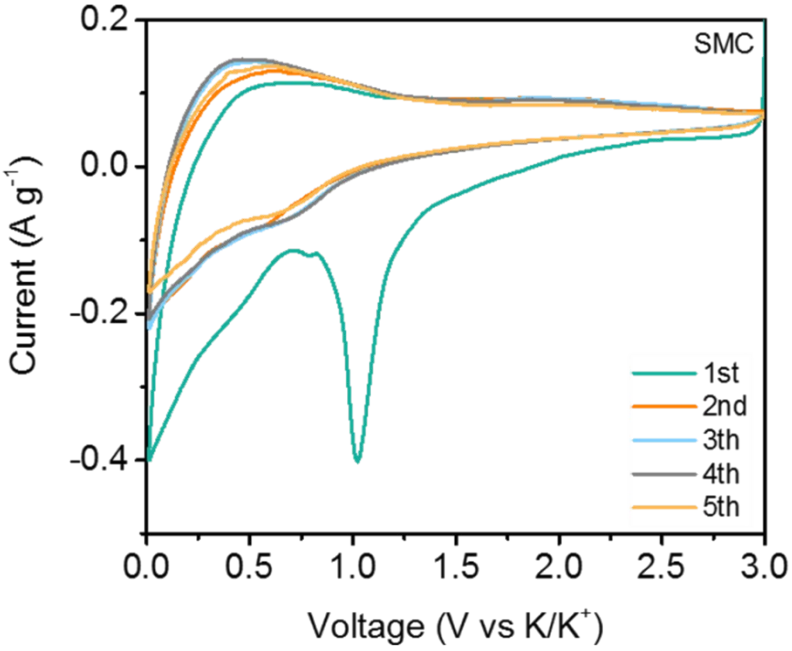

Fig. S9 CV curves of the SMC electrode at a scan rate of 0.1 mV s^{-1}

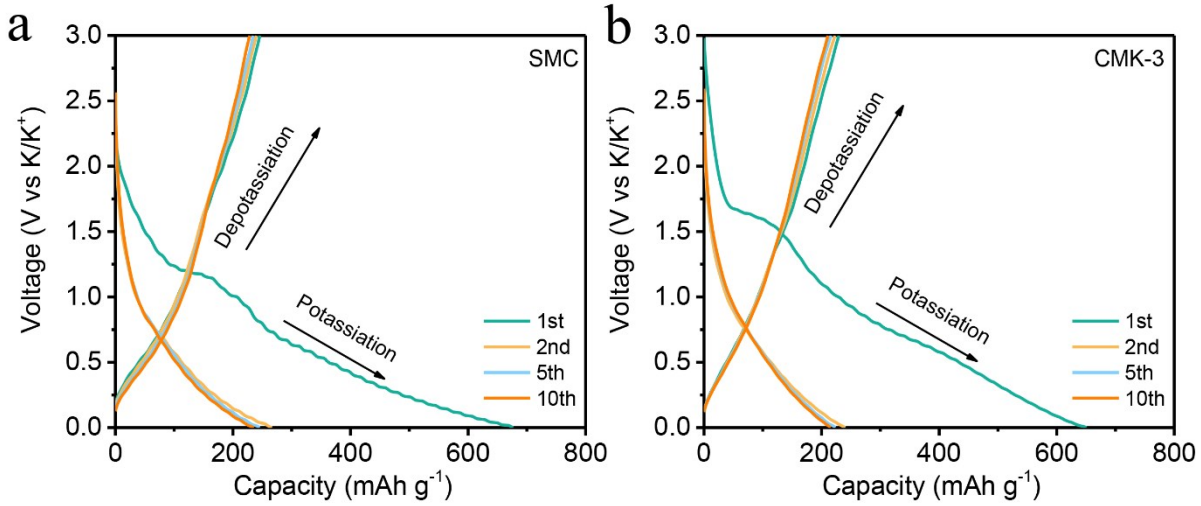

Fig. S10 Galvanostatic discharge-charge profiles at a current density of 0.1 A g^{-1} of (a) SMC and (b) CMK-3.

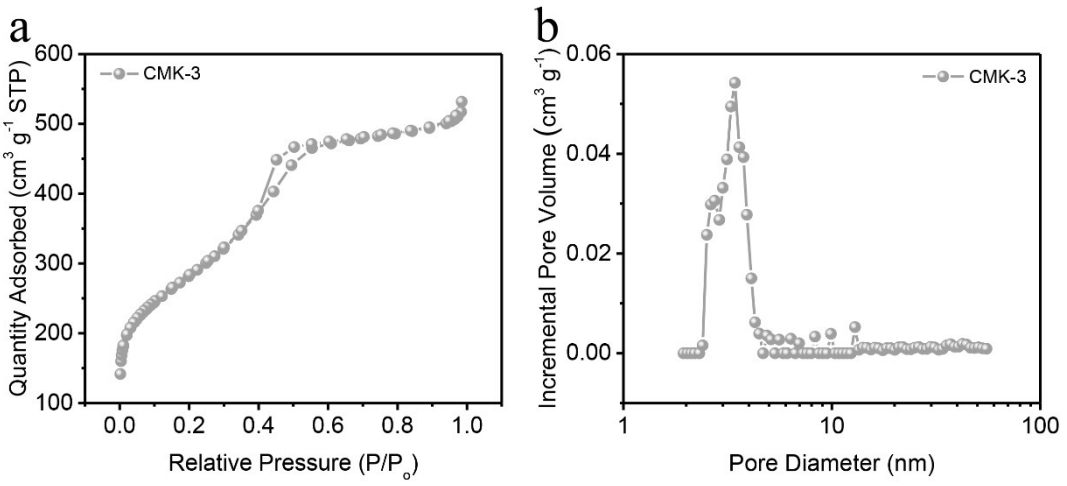

Fig. S11 (a) N_2 adsorption-desorption isotherm and (b) the corresponding DFT pore size distribution of CMK-3.

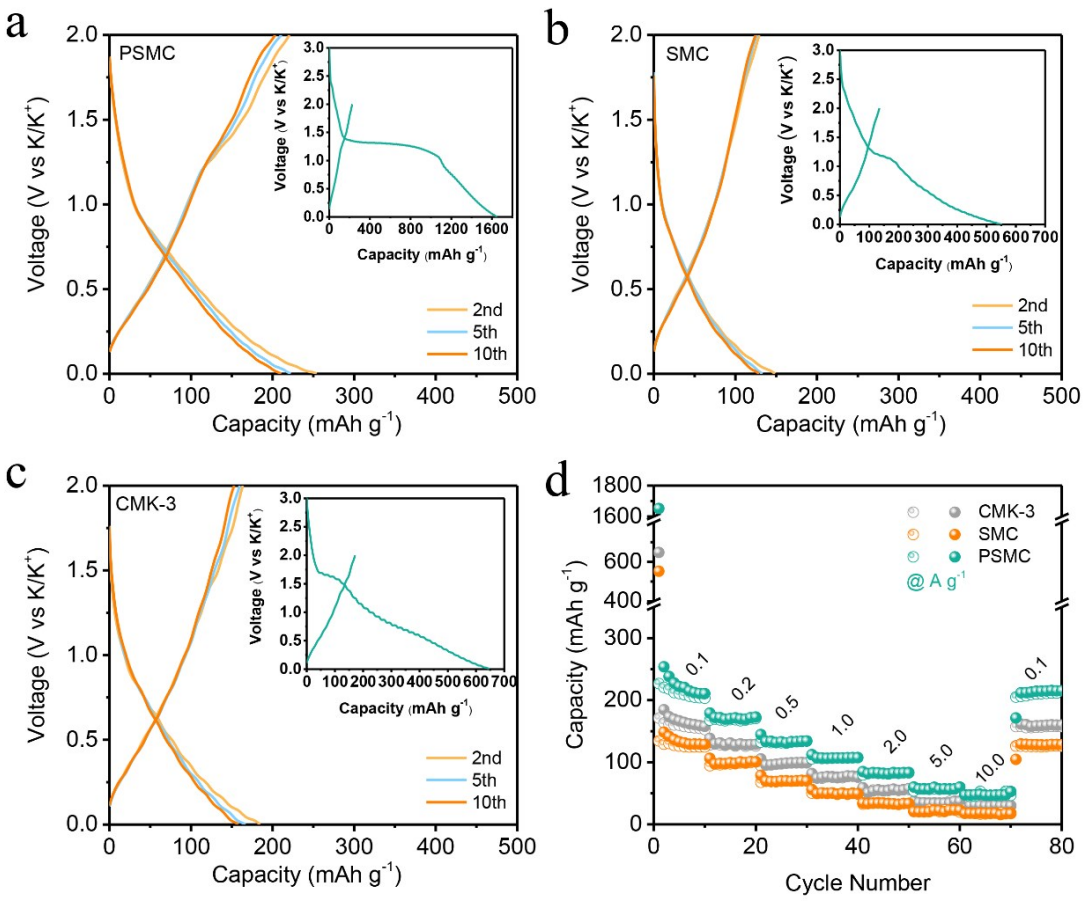

Fig. S12 Galvanostatic discharge-charge profiles of (a) PSMC, (b) SMC, (c) CMK-3 at 0.1 A g^{-1} and the cut-off voltage of 2.0 V (inset is the first cycle); (d) Rate capability of PSMC, SMC, and CMK-3.

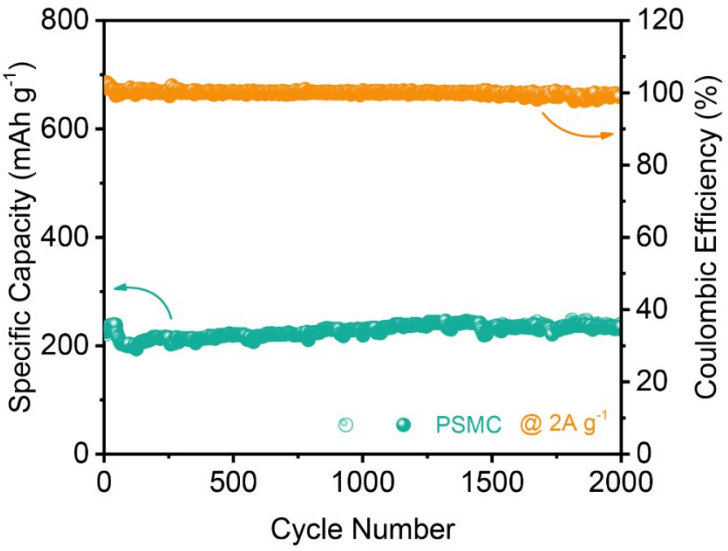

Fig. S13 Long cycling performance of PSMC at 2.0 A g^{-1}.

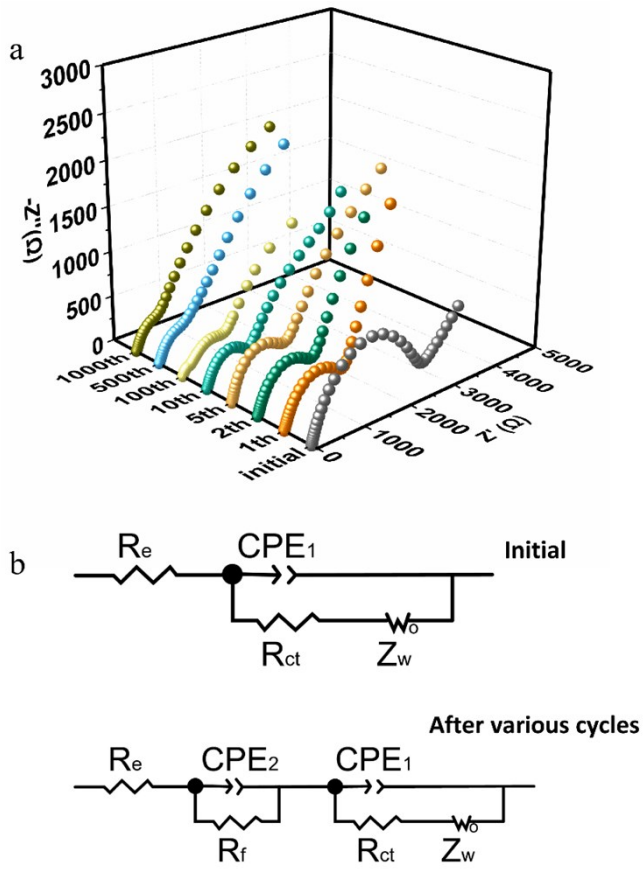

Fig. S14 (a) Nyquist plots of the SMC electrode, analyzed at initial and after various cycles. (b) The equivalent electrical circuit of the EIS fitting (R_e is the internal resistance, CPE_1 and CPE_2 are constant phase elements, R_{ct} represents charge transfer resistance, R_f represents the resistance of potassium transport through SEI layer, and Z_W is Warburg impedance).

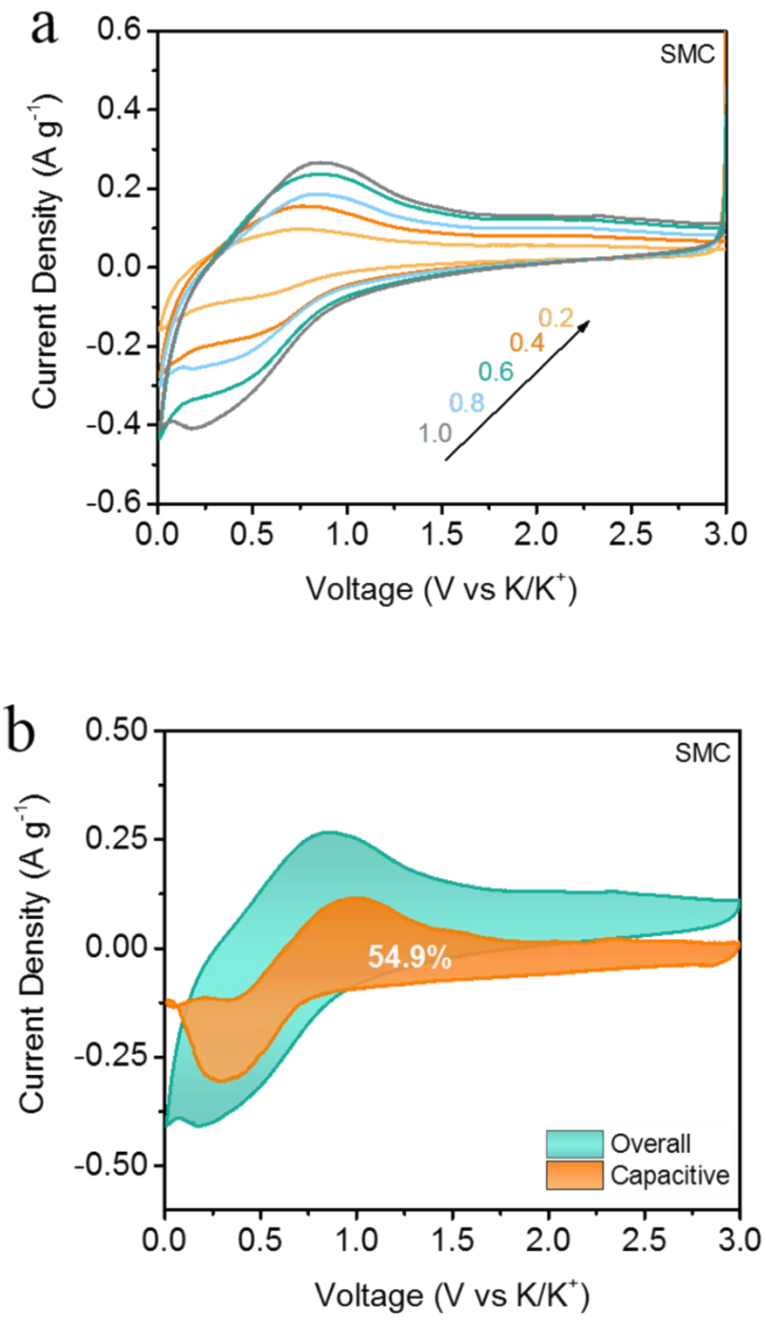

Fig. S15 (a) CV curves of SMC at various scan rates. (b) Capacitive contribution for SMC at 1.0 mV s^{-1}.

Galvanostatic intermittent titration technique (GITT)

The first cycle is tested by GCD with a current density of 0.1A g^{-1}, and the second cycle is examined by GITT. The specific test condition is to apply a constant current of 0.03 A g^{-1} pulse for 30 minutes to a PIB half-cell with PSMC/SMC as the anode, and then relax for 3 hours. The K^+ diffusion coefficients can be quantitatively calculated according to GITT curves by using the following Equation:

$$D = \frac{4}{\pi}\left(\frac{mV_B}{M_B S}\right)\left(\frac{\Delta E_s}{\Delta E_\tau}\right)^2$$

where m and M_B are the mass (g) and molar weight (g mol^{-1}) of active material, and S is the geometric contact area (cm^2) between electrolyte and electrode, V_B is the molar volume (cm^3 mol^{-1}) of active materials, and τ is current pulse duration (s). ΔE_s and ΔE_τ are the potential change in a complete pulse-elaxation procedure which can be obtained from the Figure S14.

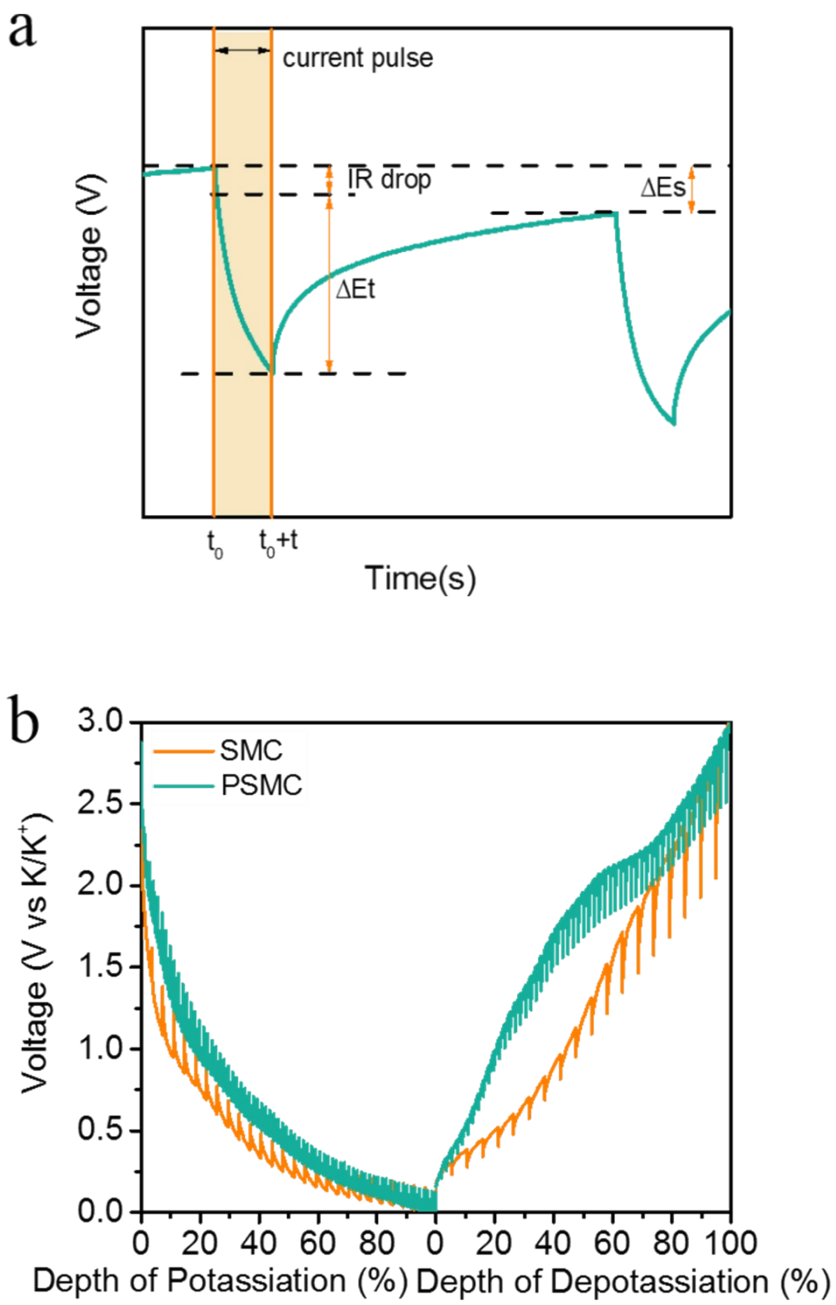

Fig. S16 (a) The schematic illustration for the GITT calculation method. (b) GITT curves for SMC and PSMC.

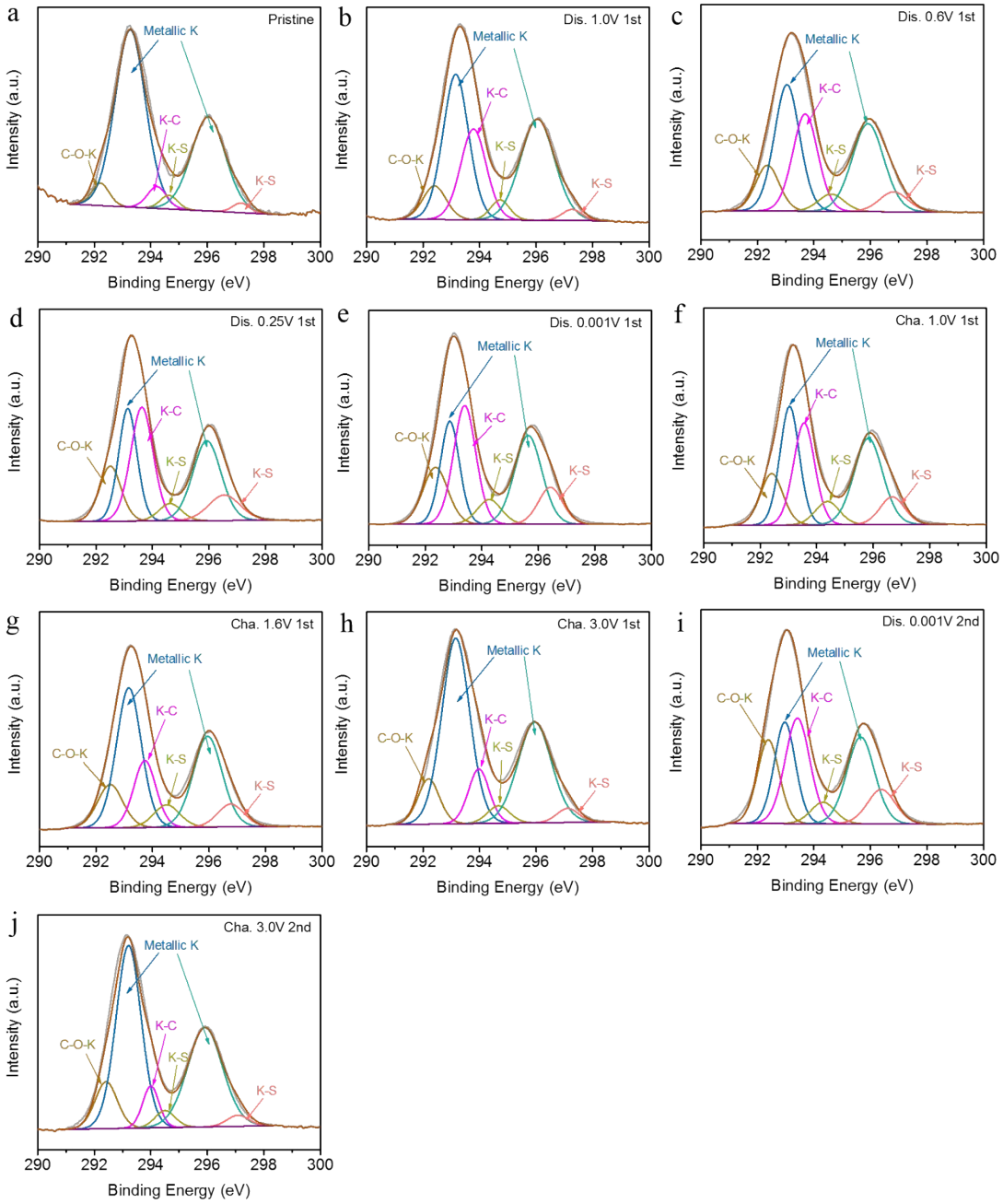

Fig. S17 Deconvolution of K 2p peaks for PSMC at various discharge/charge voltages, during cycle 1 and cycle 2: (a) pristine; (b) discharge to 1.0V (cycle 1); (c) discharge to 0.6V (cycle 1); (d) discharge to 0.25V (cycle 1); (e) discharge to 0.001V (cycle 1); (f) charge to 1.0V (cycle 1); (g) charge to 1.6V (cycle 1); (h) charge to 3.0V (cycle 1); (i)discharge to 0.001V (cycle 2); (j) charge to 3.0V (cycle 2).

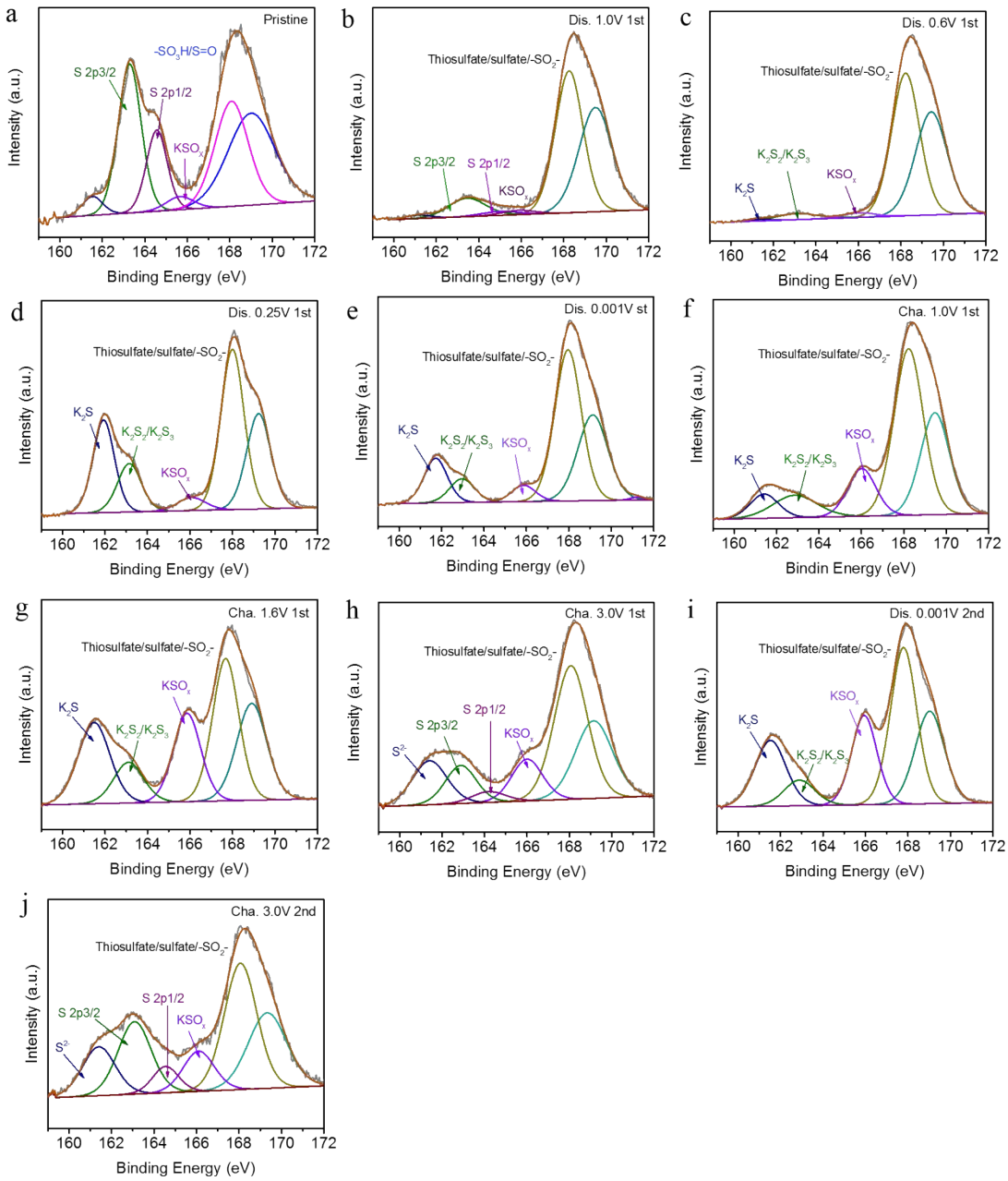

Fig. S18 Deconvolution of S 2p peaks for PSMC at various discharge/charge voltages, during cycle 1 and cycle 2: (a) pristine; (b) discharge to 1.0V (cycle 1); (c) discharge to 0.6V (cycle 1); (d) discharge to 0.25V (cycle 1); (e) discharge to 0.001V (cycle 1); (f) charge to 1.0V (cycle 1); (g) charge to 1.6V (cycle 1); (h) charge to 3.0V (cycle 1); (i)discharge to 0.001V (cycle 2); (j) charge to 3.0V (cycle 2).

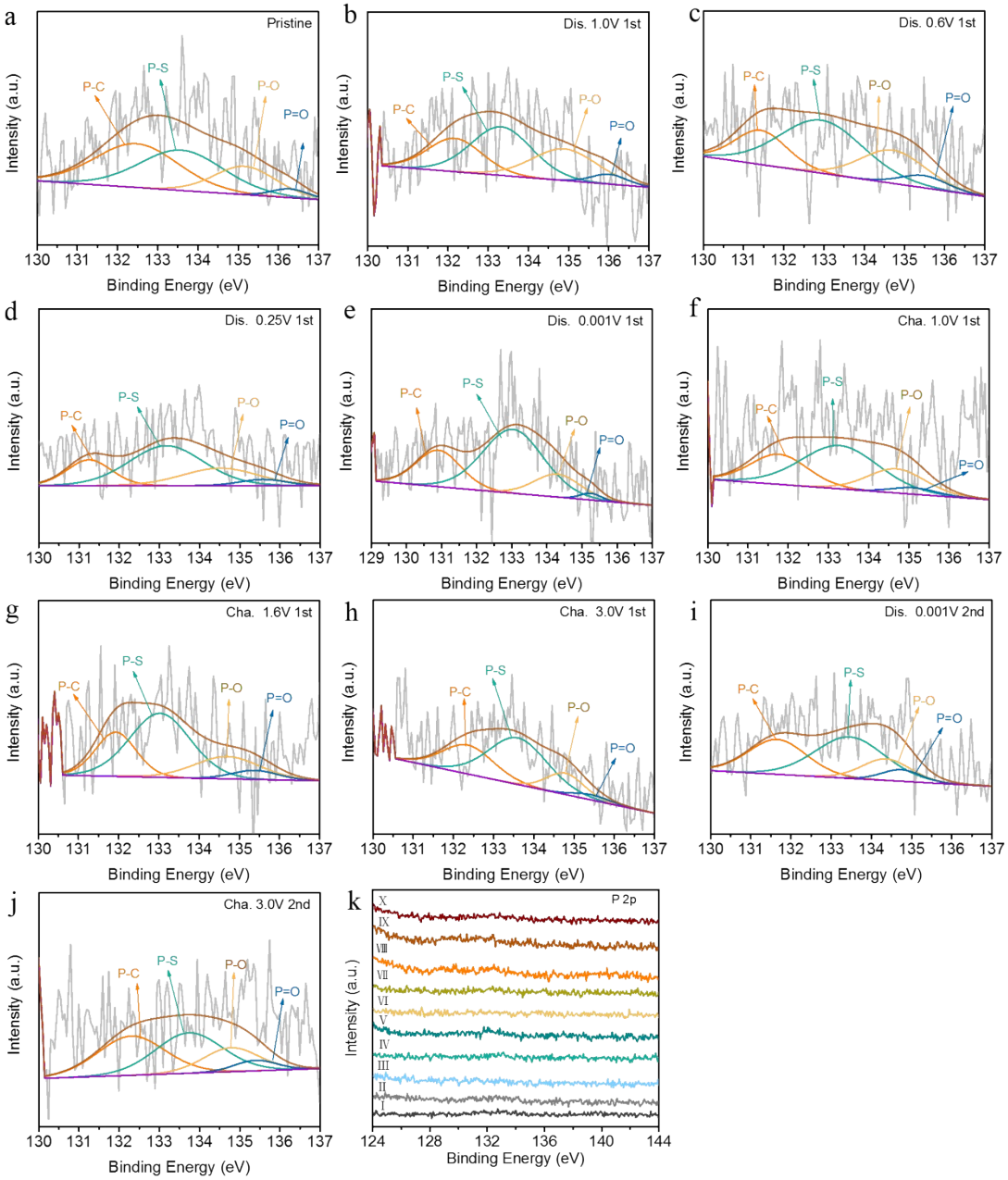

Fig. S19 Deconvolution of P 2p peaks for PSMC at various discharge/charge voltages, during cycle 1 and cycle 2: (a) pristine; (b) discharge to 1.0V (cycle 1); (c) discharge to 0.6V (cycle 1); (d) discharge to 0.25V (cycle 1); (e) discharge to 0.001V (cycle 1); (f) charge to 1.0V (cycle 1); (g) charge to 1.6V (cycle 1); (h) charge to 3.0V (cycle 1); (i)discharge to 0.001V (cycle 2); (j) charge to 3.0V (cycle 2); (k) *Ex-situ* XPS spectra of P 2p for PSMC.

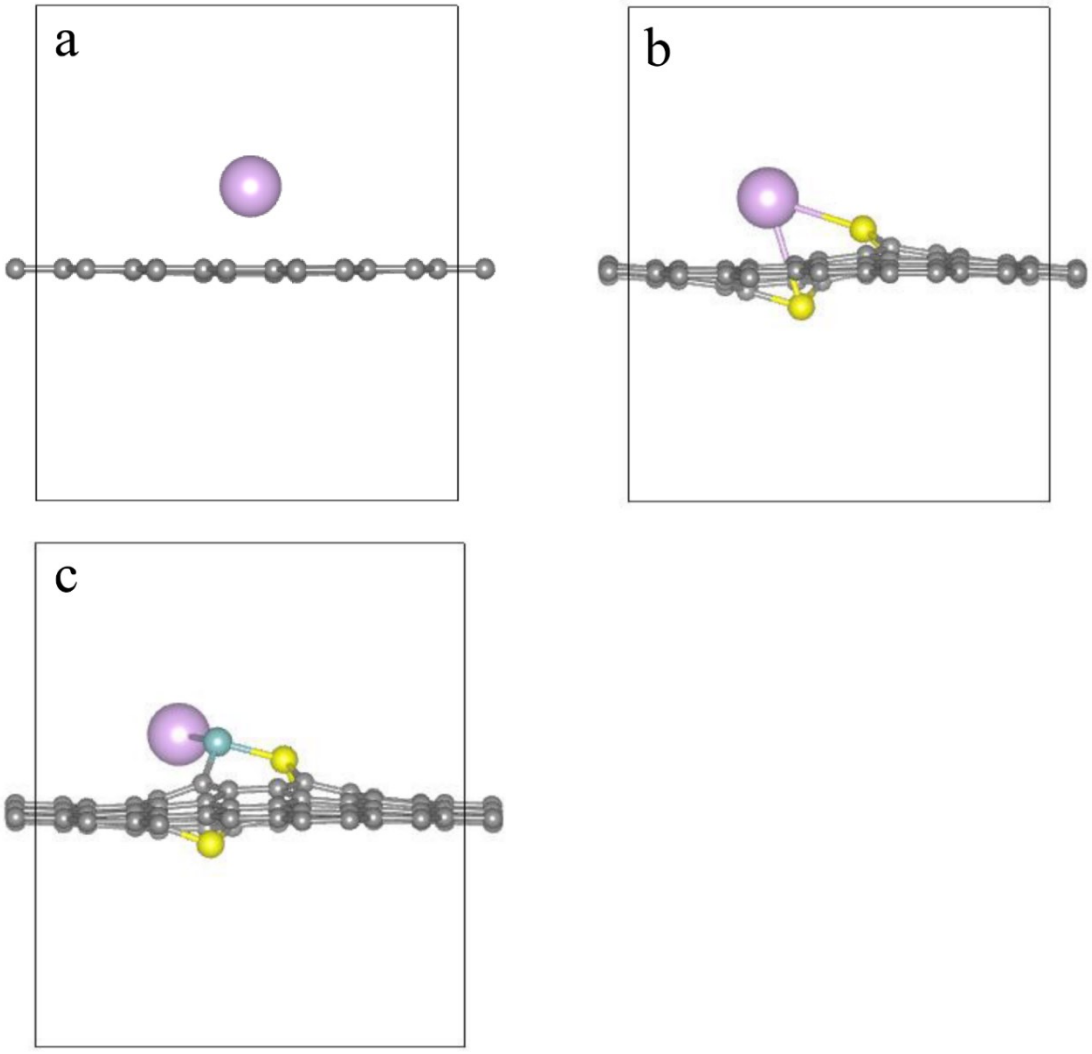

Fig. S20 Side view of the structure of (a) Graphene, (b) S-Graphene and (c) P/S-Graphene.

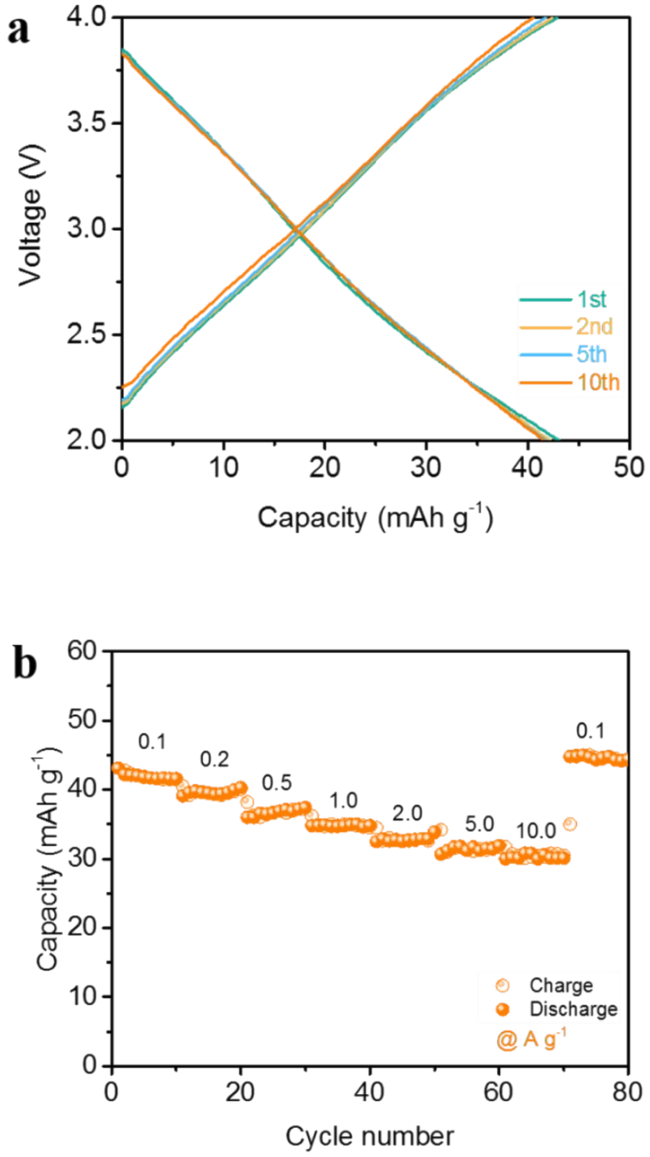

Fig. S21 Electrochemical performance of NPC as PIBs cathode in half cells. (a) Galvonastatic discharge-charge profiles of NPC at 0.1 A g^{-1}; (b) Rate capability of NPC. (The preparation process of NPC sample is as follows: Typically, 2.0 g potassium hydroxide and 10.0 g sodium bicarbonate were dissolved in deionized water, and then 2.0 g methyl cellulose and 2.0 g urea were added into the solution with continuously stirred for 4 hours. After freeze-drying, the precursor was carbonized under N_2 (200 °C for 2 hours and 800 °C for 4 hours), washed by 2M HCl and H_2O, and dried at 80 °C in vacuum oven). [2]

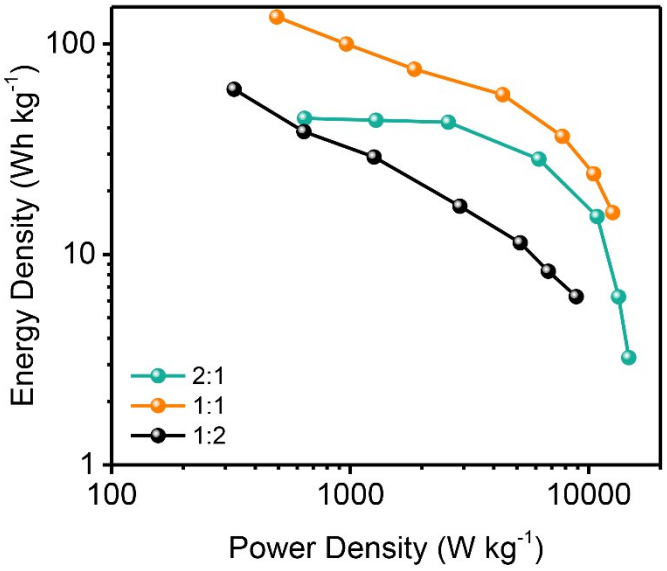

Fig. S22. Ragone plots of the PICs with different anode to cathode mass ratios (1:2, 1:1 and 2:1).

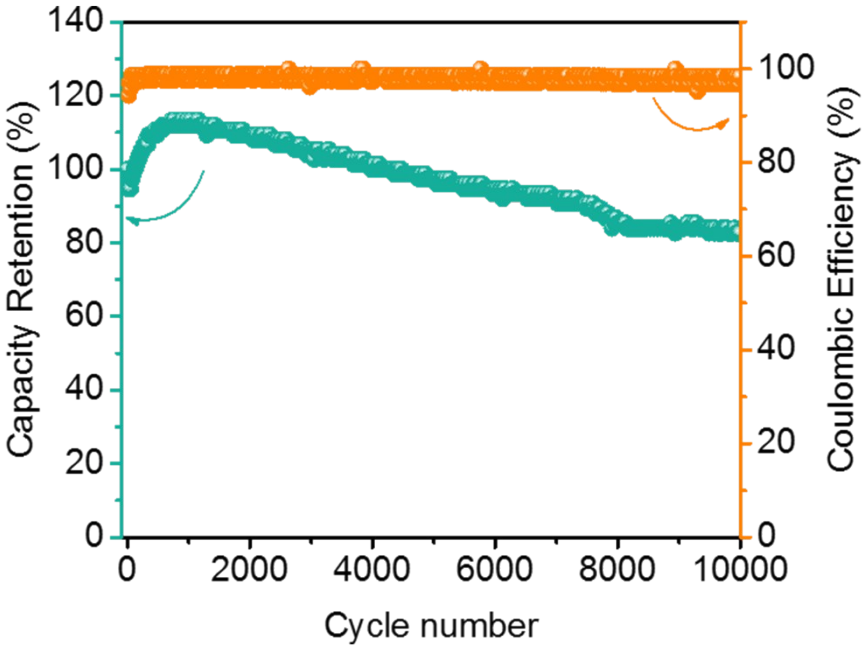

Figure S23. The long-cycle performance of PIC at 50 A g^{-1}.

Table S1. Textural properties and surface chemistry of SMC and PSMC.

Sample	Textural Properties				Surface Chemistry (XPS)				I_D/I_G
	S_{BET}	V_{total}	Pore Volume (%)		C	O	S	P	
	$m^2 \cdot g^{-1}$	$cm^3 \cdot g^{-1}$	$V_{<2nm}$	$V_{>2nm}$	wt%	wt%	wt%	wt%	
SMC	856	1.49	38.50	61.50	85.84	7.05	7.11	—	1.50
PSMC	961	3.15	12.58	87.42	76.36	6.08	16.48	1.08	1.67

Table S2. Carbon bonding analysis of SMC and PSMC samples.

Binding Energy (eV)	Carbon Bonding	Concentration (%/at %)	
		SMC	PSMC
284.4	C=C	48.62/44.50	46.07/40.20
285.0	C-C	20.29/18.57	24.49/21.37
285.8	C-S	9.27/8.48	12.44/10.86
286.8	C-O	8.61/7.88	6.60/5.76
289.3	C=O	13.21/12.09	9.19/8.02
283.4	C-P	—	1.20/1.05
$Sp^2/(Sp^2+Sp^3)$		70.56	65.29

Table S3. Comparisons of electrochemical performance of PSMC with other carbon anodes for PIBs.

Anode Materials	Rate capability	Cycling Performance
PSMC (This work)	**449 mAh g^{-1} at 0.1 A g^{-1},** **407 mAh g^{-1} at 0.2 A g^{-1},** **355 mAh g^{-1} at 0.5 A g^{-1},** **299 mAh g^{-1} at 1.0 A g^{-1},** **233 mAh g^{-1} at 2.0 A g^{-1},** **136 mAh g^{-1} at 5.0 A g^{-1}** **98 mAh g^{-1} at 10.0 A g^{-1}**	**217.1 mAh g^{-1} after 1000 cycles at 2 A g^{-1}**
CFM-S30NG [3]	306.8 mAh g^{-1} at 0.05 A g^{-1}, 279.2 mAh g^{-1} at 0.1 A g^{-1}, 269.1 mAh g^{-1} at 0.2 A g^{-1}, 245.0 mAh g^{-1} at 0.5 A g^{-1}, 222.7 mAh g^{-1} at 1.0 A g^{-1}	188.8 mAh g^{-1} after 200 cycles at 1 A g^{-1}
S-RGO-600 [4]	435 mAh g^{-1} at 0.05 A g^{-1}, 297 mAh g^{-1} at 0.1 A g^{-1}, 282 mAh g^{-1} at 0.25 A g^{-1}, 250 mAh g^{-1} at 0.5 A g^{-1}, 224 mAh g^{-1} at 1.0 A g^{-1}	229 mAh g^{-1} after 500 cycles at 1 A g^{-1}
S/NCNFAs [5]	356 mAh g^{-1} at 0.1 A g^{-1}, 260 mAh g^{-1} at 0.2A g^{-1}, 220 mAh g^{-1} at 0.5 A g^{-1}, 198 mAh g^{-1} at 1.0 A g^{-1}, 168 mAh g^{-1} at 2.0 A g^{-1}, 112 mAh g^{-1} at 5.0 A g^{-1},	168 mAh g^{-1} after 1000 cycles at 2 A g^{-1}
CNFF [6]	240 mAh g^{-1} at 0.05 A g^{-1}, 236 mAh g^{-1} at 0.08A g^{-1},	141 mAh g^{-1} after 2000 cycles at 1 A g^{-1}

	214 mAh g^{-1} at 0.1 A g^{-1}, 202 mAh g^{-1} at 0.2 A g^{-1}, 181 mAh g^{-1} at 0.5 A g^{-1}, 164 mAh g^{-1} at 1.0 A g^{-1},	
H-OS-C [7]	409 mAh g^{-1} at 0.1 A g^{-1}, 322 mAh g^{-1} at 0.2 A g^{-1}, 255 mAh g^{-1} at 0.5 A g^{-1}, 185 mAh g^{-1} at 1.0 A g^{-1}, 135 mAh g^{-1} at 2.0 A g^{-1}	120 mAh g^{-1} after 500 cycles at 2 A g^{-1}
CAPC1100 [8]	233.7 mAh g^{-1} at 0.5 A g^{-1}, 208.7 mAh g^{-1} at 1.0 A g^{-1}, 196.6 mAh g^{-1} at 1.5 A g^{-1}, 189.7 mAh g^{-1} at 2.0 A g^{-1} 177.3 mAh g^{-1} at 2.5 A g^{-1}	171.5 mAh g^{-1} after 500 cycles at 1.5 A g^{-1}
NOC@GF [9]	340 mAh g^{-1} at 0.1 A g^{-1}, 329 mAh g^{-1} at 0.2 A g^{-1}, 306 mAh g^{-1} at 0.5 A g^{-1}, 287 mAh g^{-1} at 0.8 A g^{-1}, 272 mAh g^{-1} at 1.0 A g^{-1}, 186 mAh g^{-1} at 2.0 A g^{-1}, 151 mAh g^{-1} at 3.0 A g^{-1}, 134 mAh g^{-1} at 4.0 A g^{-1}, 123 mAh g^{-1} at 5.0 A g^{-1},	281 mAh g^{-1} after 5500 cycles at 1.0 A g^{-1}
SC-500 [10]	175 mAh g^{-1} at 0.05 A g^{-1}, 150 mAh g^{-1} at 0.1 A g^{-1}, 118 mAh g^{-1} at 0.2 A g^{-1}, 93 mAh g^{-1} at 0.4 A g^{-1}, 70 mAh g^{-1} at 0.8 A g^{-1},	196 mAh g^{-1} after 900 cycles at 0.05 A g^{-1}

CDs @ rGO [11]	309 mAh g^{-1} at 0.1 A g^{-1}, 270 mAh g^{-1} at 0.2 A g^{-1}, 250 mAh g^{-1} at 0.3 A g^{-1}, 227 mAh g^{-1} at 0.4 A g^{-1}, 221 mAh g^{-1} at 0.5 A g^{-1},	244 mAh g^{-1} after 840 cycles at 0.2 A g^{-1}
KTO/C-700 [12]	122.5 mAh g^{-1} at 0.02 A g^{-1}, 104.3 mAh g^{-1} at 0.05 A g^{-1}, 92.3 mAh g^{-1} at 0.1 A g^{-1}, 78.6 mAh g^{-1} at 0.2 A g^{-1}, 65.1 mAh g^{-1} at 0.5 A g^{-1},	118.5 mAh g^{-1} after 200 cycles at 0.025 A g^{-1}

References

1 D. Li, Y. Jia, G. Chang, J. Chen, H. Liu, J. Wang, Y. Hu, Y. Xia, D. Yang and X. Yao, *Chem*, 2018, **4**, 2345-2356.

2 Y. Cui, W. Liu, Y. Lyu, Y. Zhang, H. Wang, Y. Liu and D. Li, *J. Mater. Chem. A*, 2018, **6**, 18276-18285.

3 W. Yang, J. Zhou, S. Wang, Z. Wang, F. Lv, W. Zhang, W. Zhang, Q. Sun and S. Guo, *ACS Energy Lett.*, 2020, **5**, 1653-1661.

4 J. Li, W. Qin, J. Xie, H. Lei, Y. Zhu, W. Huang, X. Xu, Z. Zhao and W. Mai, *Nano Energy*, 2018, **53**, 415-424.

5 C. Lv, W. Xu, H. Liu, L. Zhang, S. Chen, X. Yang, X. Xu and D. Yang, *Small*, 2019, **15**, e1900816.

6 H. Li, Z. Cheng, Q. Zhang, A. Natan, Y. Yang, D. Cao and H. Zhu, *Nano Lett.*, 2018, **18**, 7407-7413.

7 B. Xu, S. Qi, F. Li, X. Peng, J. Cai, J. Liang and J. Ma, *Chin. Chem. Lett.*, 2020, **31**, 217-222.

8 B. Wang, F. Yuan, W. Li, Q. Wang, X. Ma, L. Gu, H. Sun, K. Xi, D. Zhang and W. Wang, *Nano Energy*, 2020, **75**, 104979.

9 S. Zeng, X. Chen, R. Xu, X. Wu, Y. Feng, H. Zhang, S. Peng and Y. Yu, *Nano Energy*, 2020, **73**, 104807.

10 L. Tao, L. Liu, R. Chang, H. He, P. Zhao and J. Liu, *J. Power Sources*, 2020, **463**, 228172.

11 E. Zhang, X. Jia, B. Wang, J. Wang, X. Yu and B. Lu, *Adv. Sci.*, 2020, **7**, 2000470.

12 C. Liu, H. Wang, S. Zhang, M. Han, Y. Cao, S. Liu, Z. Yang, A. Chen and J. Sun, *Nanoscale*, 2020, **12**, 11427-11434.